Modification to axial tracking for mobile magnetic microspheres

Laura A Carlucci<sup>1</sup> and Wendy E Thomas<sup>1\*</sup>

<sup>1</sup>Department of Bioengineering, University of Washington, Seattle, Washington, 98195, USA

\*For correspondence: wendyt@uw.edu

#### **Abstract**

Three-dimensional particle tracking is a routine experimental procedure for various biophysical applications including magnetic tweezers. A common method for tracking the axial position of particles involves the analysis of diffraction rings whose pattern depends sensitively on the axial position of the bead relative to the focal plane. To infer the axial position, the observed rings are compared with reference images of a bead at known axial positions. Often the precision or accuracy of these algorithms is measured on immobilized beads over a limited axial range, while many experiments are performed using freely mobile beads. This inconsistency raises the possibility of incorrect estimates of experimental uncertainty. By manipulating magnetic beads in a bidirectional magnetic tweezer setup, we evaluated the error associated with tracking mobile magnetic beads and found that the error of tracking a moving magnetic bead increases by almost an order of magnitude compared to the error of tracking a stationary bead. We found that this additional error can be ameliorated by excluding the center-most region of the diffraction ring pattern from tracking analysis. Evaluation of the limitations of a tracking algorithm is essential for understanding the error associated with a measurement. These findings promise to bring increased resolution to three-dimensional bead tracking of magnetic microspheres.

# Why It Matters

Tracking a particle in three dimensions under a microscope is a routine experimental procedure. Tracking a particle as it moves up or down relative to the microscope objective though, is not as simple as tracking the particle's left/right movements and tends to have a higher error. To estimate this error, most methods track simulated beads or immobilized beads. We estimate the error by tracking moving beads and find the error is much higher than found by other means. We suspect this is because the slight bead irregularities interfere with the position estimation when beads rotate. Therefore, it is important to consider the additional impact of bead motion when tracking bead positions.

#### Introduction

Three-dimensional tracking of microspheres (often simply called beads) is useful in various biological fields to study processes as diverse as bacterial motion<sup>1</sup>, opening and closing of a DNA hairpin<sup>2</sup>, protein unfolding<sup>3</sup>, and chromosomal motion<sup>4</sup>. and plays an important role in various biophysical techniques including optical trap<sup>5</sup>, centrifugal force spectroscopy<sup>6</sup>, and traction force microscopy<sup>7</sup>. Bead tracking in the z- or axial direction (perpendicular to the focal plane) is particularly important for magnetic tweezer use<sup>8</sup>. Magnetic tweezers apply forces on molecular interactions through the usage of magnetic beads and magnets. In many magnetic tweezer experiments, the movements of the magnetic beads are monitored through the objective of an inverted microscope and recorded with a high-speed camera. Magnetic beads have high variability in magnetism and thus force must be calibrated for each individual bead<sup>9</sup>. The movement of the magnetic bead along the axial direction can be used to calculate the force on a bead and therefore on the molecules attached to the bead<sup>10,11</sup>.

Although many methods provide robust sub-pixel resolution of lateral positions <sup>12,13</sup>, tracking in the axial direction requires a different approach with unique challenges. Optical tweezers utilize quadrant-photodiode tracking in which the 3D position of a trapped particle is estimated from laser light scattered off the bead <sup>12</sup>. However, this method can only track one bead at a time. In contrast, two camera-based tracking techniques <sup>6,14</sup> can determine the z-positions of multiple beads simultaneously. One technique uses holographic tracking microscopy and Mie scattering theory. Holographic images are generated from light scattered by a particle and fit with the Lorenz-Mie scattering theory to estimate the distance the particle is from the focal plane with nanometer resolution <sup>15</sup>. Another common technique involves utilizing a Look Up Table (LUT) of off-focus images generated by moving a microscope objective or piezo stage and taking images of a bead at evenly spaced intervals over an axial range. The pattern of diffraction rings around the off-focus bead is used to generate a radial profile for each bead which corresponds to a known distance from the objective. The radial profile of a bead at an unknown position is compared to the LUT and inter-step z-position is inferred via interpolation of the steps in the LUT<sup>14</sup>.

Although in principle each of these methods can provide up to subnanometer-level resolution  $^{6,16}$ , several factors affect the accuracy of tracking moving beads in the axial direction. First, it has been previously demonstrated that low nanometer-level precision only occurs within a narrow region near the focal plane  $^{14,17,18}$ . Many 3D bead tracking methods typically explore a range of no more than  $20~\mu m^{14}$ . The accuracy of tracking varies greatly even within this range and the optimal axial range spans just a few microns  $^{14}$ . A distance of a few microns is sufficient when estimating the unfolding of proteins  $^{3,19,20}$ . However this distance is insufficient when using long linkers such as bacterial fimbria  $^{21}$  or long DNA  $^{22}$ , or when tracking large movements of an untethered bead  $^{10,21}$ . For applications that require tracking a magnetic bead over tens of microns, overall tracking accuracy decreases.

A second potential mechanism for generating tracking errors is that a bead may move during acquisition of a single image, leading to blurring of the bead. In theory, movement within the lateral plane or in the axial direction might distort the radial profile.

A third mechanism for the loss of tracking precision involves the non-uniformity of the beads themselves contributing to poor tracking accuracy. Bead imperfections are known to interfere with holographic tracking due to their inability to fit Lorenz-Mie scattering theory well<sup>17</sup>. LUT tracking utilizes reference images, typically taken from the same bead of interest while not moving. It has been shown that the polydispersity of beads results in significantly higher error when the LUT is generated from a different bead compared to the same bead of interest<sup>23</sup>. As an asymmetric bead rotates, the diffraction pattern of the bead may be as dissimilar to the originally viewed pattern as that of a different bead. These concerns raise the question of whether the precision of the LUT method would also be sensitive to focal distance, bead blurring, or rotation of non-uniform mobile beads.

The impact of bead movement is not addressed by common methods of calibrating the accuracy or precision of a tracking algorithm, including using simulated bead images with added noise 13,18,24,25, tracking a bead that is non-specifically adsorbed onto a surface when the microscope stage is stationary 2,26,27 or moving 2,14,17, or tracking the z-positions of a tethered magnetic bead held taut under a magnetic field 18. It therefore remains necessary to evaluate to what degree bead movement contributes to error in LUT tracking algorithms.

In this work, we explore the precision of tracking of freely moving beads over an axial distance of almost  $100 \mu m$ , compared to stuck beads, for a tracking method based on the

algorithm described by Van Loenhout et al. 16 that utilizes quadrant interpolation and a LUT. As expected, we found that the combination of free movement of a bead, along with the larger tracking distance, resulted in a relatively large standard deviation of estimated positions compared to immobilized beads. We also test and optimize modifications in the tracking algorithm that reduce the impact of bead mobility. We found that part of the error associated with mobile beads could be rectified by excluding pixels corresponding to the center of the bead when evaluating the z-position from the LUT. These modifications will greatly increase the precision of tracking and improve the estimation of the error of the tracking algorithm of a freely moving bead over a large axial distance.

#### Methods

Chamber construction

Chambers were constructed as described in Johnson et al. 2017. Briefly, chamber slides (Fisherbrand Microscope Cover Glass,  $24 \times 60 \times 1.5$ , Fisher Scientific) were rinsed with 70% ethanol and dried. Chambers were assembled with double sided sticky tape and injected with approximately 80  $\mu$ L of 0.2% PBS-BSA (Sigma, Cat # A3059). Chambers were covered and stored overnight at 4°C.

# Magnetic microbeads

Magnetic beads were diluted 100-fold in 0.2% PBS-BSA. Unless specified, the magnetic beads used were 8.3 μm diameter (Compel Magnetic Microspheres COOH modified, Bangs Laboratories Inc., Cat# UMC4001). Other beads used were 2.8 μm diameter (Dynabeads M-280 Streptavidin, Thermo Fisher Scientific Cat# 11205D), 5.8 μm diameter (Streptavidin Coated Compel Magnetic Microspheres, Bangs Laboratories Inc., Cat# UMC0101), 8.8 μm diameter (Carboxyl Magnetic Particles, Spherotech Cat# CM-80-10), 11.0 μm diameter (Carboxyl Magnetic Particles, Spherotech Cat# CM-100-10).

# Chambers with Nonspecifically Bound Beads

Beads were nonspecifically bound to a slide by adding 100  $\mu$ L of beads diluted 100-fold in water in the center of a cleaned slide. The slide was heated at 37°C until all liquid evaporated. Slides were rinsed with PBS and chamber was constructed as described above. The size of the chambers typically ranged 60-80  $\mu$ m in height (as measured by the difference in ceiling and floor axial position).

### Magnetic Tweezer usage

A magnetic tweezers with bidirectional force control was used as described in Johnson et al.  $^{10}$  with a 0.45 NA 20x objective installed (Figure 1A). Unless otherwise specified, the axial position was set so that the chamber floor was approximately 50  $\mu$ m away from the focus. At the start of each run, 20  $\mu$ L of diluted beads were injected into the chamber and allowed to settle. The upper magnets were turned on with a voltage of 40 V and 0.1 amps for one second, after which the lower magnets were turned on with 40 V and 5 amps for 4 seconds. The upper and lower magnets were alternately turned on 2 more times each at the same current and voltage. One second separated the switch between each set of magnets to ensure both magnets were never on simultaneously. Bead images were recorded at 18 frames per second.

Because the 5.8 and 2.8  $\mu m$  beads were lower in mass than the larger 8.3  $\mu m$  beads and move slower under the same magnetic field, the lower magnets remained on for a total of 6 seconds to ensure the majority of beads encountered the bottom surface and the frame rate was reduced to 15 frames per second.

Immobilized beads were tracked at 18 frames per second for a total of 4 seconds while the beads were on the chamber floor. The chamber was then flipped upside down so that the immobilized beads were on the chamber surface and the beads were tracked in the same way as when they were on the floor.

### Bead Tracking

#### Lateral bead tracking

Beads were tracked with a method based on quadrant interpolation from Van Loenhout et al<sup>16</sup>. In short, using a custom MATLAB script<sup>28</sup> (MathWorks, Natick, MA) initial estimates of the coordinates of a bead were input by the user. A square cutout of the image was taken surrounding the input coordinates. The image cutout is then rotated 90° and the fast Fourier transform of both the original and rotated images were taken. The pixel shift needed to align the Fourier transform of both images was used to estimate by how many pixels the input coordinates were off from the true bead center. Subsequent images were calculated as thus, using the calculated bead center from the previous frame as the starting coordinates as the initial guess of the bead centroid.

### Axial bead tracking

Tracking along the z-axis was based upon Zhang et al., Van Loenhout et al., and Johnson et al. <sup>10,14,16</sup>. As the beads moved in and out of focus, the diffraction ring patterns around the beads change. This pattern was compared to the diffraction ring patterns of calibration beads by reducing the grey-scale bead image to a radial profile. Bead images were background subtracted to account for gradients in light. Radii were drawn from the center of the bead (as calculated in the above section) evenly spaced around a bead. The pixel intensities at each position along these radii were calculated and averaged together to create a single radial profile for each frame for each bead (Figure 1B). As the bead images were background subtracted, pixels darker than the background have a negative intensity. These radial profiles were compared to a LUT, generated in a similar manner using calibration images. To minimize error associated with bead-to-bead variation, each LUT was customized to be the average of the radial profiles of 5 calibration beads that most closely match the analysis bead, further described below. Z-positions of a bead in each frame were estimated by finding the radial profile in the averaged LUT stack with the lowest root mean square error (RMSE). To obtain a resolution smaller than the step size of the LUT, the radial profiles were interpolated using a cubic-spline.

#### LUT generation

A z-stack of a field of calibration beads was collected with images taken at a range starting from an approximate 'in-focus' plane and ending 200  $\mu$ m below this focus at 2  $\mu$ m intervals for a total of 100 images. Each bead in the field of view was processed to create a separate LUT. Upon analysis of the first frame of an analysis bead in a video, the analysis bead is compared to the LUT of each calibration bead to find the closest matching radial profile. The root mean square error between the closest radial profile of each calibration bead and the radial profile of the analysis bead was calculated. The five calibration beads with the lowest associated

error were identified as the ones most similar to the analysis bead. The radial profiles of these LUT were averaged together for each 2 µm step to generate a composite LUT that was used to calculate axial position of the analysis bead. Using this averaging approach reduces bead-to-bead variability and ensures one calibration bead is not biasing the analysis method. A new averaged reference stack was generated for each analysis bead and used to track the bead through the entire video from the array of LUTs. A different field of calibration beads was collected for beads of each size but the same field of calibration beads was used for all beads of the same size analyzed in this work.

# Estimation of chamber floor and ceiling

Due to variations in the magnetism of the beads, each bead moved with a different velocity and thus required different amounts of time to traverse the chamber and reach the opposite surface. The first frame in which a bead reached the surface was estimated as either when the difference between two consecutive axial positions was the opposite sign as the immediately preceding difference in positions or when the magnitude of the next five differences in axial position were each below 250 nm. The moment the bead leaves a surface can be determined from the time the opposing magnetic field is switched on.

## Estimation of bead velocity

Velocities were calculated from the downward (towards chamber floor) movement of the beads. As each bead was subjected to three up/down pulls, there were three instances in which the velocity was measured for each bead. Only z-positions that fell within the middle third region of the chamber were used to estimate the bead velocity to equalize the influence of the chamber surfaces on the moving particle. Since our chambers were about 70  $\mu$ m in height, this middle third region tended to range from 23  $\mu$ m above the chamber floor to 23  $\mu$ m below the chamber ceiling. The positions used to calculate a single velocity estimation were identified as the consecutive points that fell within this middle region. The velocity of the bead through these points was then determined by finding the least-squares solution of a linear fit (y = mx+b) to the identified consecutive points, in which y is the bead position, and x is time in seconds. The absolute value of the slope of the line (m) was taken to be the velocity. This calculation is repeated for each of the three sections of consecutively decreasing positions of a bead to obtain three downward velocities per bead. The fractional standard deviation of the velocities is reported to normalize the error between beads. This was found by taking the standard deviation of the three velocities divided by the average of the three velocities.

### Statistical analysis

Confidence intervals were determined by and all statistical analysis was performed using GraphPad Prism 9 (San Diego, CA). As the distribution of errors was not normal, nonparametric tests were used. When comparing immobilized to mobile beads (in Figure 2) the Kruskal-Wallis test, followed by Dunn's multiple comparison test was used. A total of 90 immobilized beads on the floor over 10 videos and 79 immobilized on the ceiling over another 10 videos were collected in one day. These were compared to mobile 8.3 µm beads.

When comparing the various analysis methods, pairwise analyses were performed as the data sets were generated from the same beads. When comparing three or more data sets (as in Figure 4), a Friedman test was first used to identify whether there was any difference in the groups, followed by Dunn's multiple comparison test to determine how each method compared

to the others. When comparing just two data sets (as in Figures 5 and 6), the Wilcoxon signed rank test was used. Only beads that stayed in the field of view and thus could be tracked through three successive up/down pulls were kept, resulting in a total of 223 beads across 44 videos collected on three separate days for the 8.3  $\mu$ m beads. An additional 31 8.3  $\mu$ m beads were collected at 10  $\mu$ m away from the focus across 10 videos in one day. 151 2.8  $\mu$ m beads across 12 videos in one day were collected. 89 5.8  $\mu$ m, 136 8.8  $\mu$ m, and 93 11  $\mu$ m beads were collected across 15 videos each in one day.

#### Results

To measure the precision of our tracking algorithm on a dynamic bead, magnetic beads were manipulated in a bidirectional magnetic tweezer set up (Figure 1A). Magnetic 8.3 µm diameter beads (Bangs Laboratories) were tracked in the z-axis by reducing the pattern of diffraction rings around the bead to a radial profile, which was compared to a LUT of similar profiles collected from calibration beads at known axial positions (Figure 1B). To increase throughput, a single field of view containing 27 reference beads was used to create a collection of LUTs to calculate axial positions for all beads of the same size. To minimize error due to the bead-to-bead variation, each bead was analyzed using a composite LUT made up of the 5 reference beads most similar to that experimental bead.

To assess tracking error in the absence of bead movement, we first measured the precision of the tracking algorithm with beads immobilized on the chamber ceiling or floor. The standard deviation ( $\sigma$ ) of all positions for a bead reflects the precision. With the beads on the floor the standard deviation was found to be 0.1  $\mu$ m. As expected, the precision decreased when the beads were on the ceiling, to a standard deviation of 0.25  $\mu$ m.

A field of beads was exposed to 3 successive rounds of repeated up/down pulls with one second pauses between each pull. Beads were pulled up with a force stronger than the force pulling them down. An axial position vs time graph of a bead gives some indication about the quality of a bead track. We would expect the bead to appear to alternate between the chamber ceiling and floor with distinct 'flat' regions in which the bead stops moving. The 'flat' regions corresponding with the floor or ceiling should be in approximately the same z-location as the bead returns to the same surface after each pull. We noticed great variability in how well certain beads were tracked using this method. Some axial position vs time graphs show the bead moving as expected (Figure 2A). However, the axial position vs time graphs of other beads had obvious artifacts, such as inconsistencies in the location of the ceiling or fluctuations in the location of the ceiling or floor (Figure 2B). The fluctuations in positions at the floor at frames 80 and 232 were associated with rolling of the bead across the chamber floor in the lateral direction due to the slightly asymmetric magnetic field. At frame 232 the bead appears to rotate, which coincides with the bottom magnets turning off. This video is included in the Supplemental material. The axial positions of the surfaces should be fairly consistent across the chamber, and no irregularities are observed on the chamber floor or ceiling that could explain the observed jumps in axial position. These observations suggest that rotation combined with lateral movement of the beads in relation to the objective, may result in the observed tracking errors.

We next quantified the precision of tracking mobile beads. We refer to each time the bead remains on one of the surfaces as a dwell. Each dwell lasted at least one full second (or 18 frames) but often longer, depending on the time needed for the bead to traverse the length of the chamber. To estimate the precision for tracking a bead held against a surface by a magnetic field, we calculated the standard deviation of all axial positions for the timepoints of each dwell.

Unlike immobilized beads, beads held to a surface by a magnetic field are free to rotate or move laterally. These precisions decreased significantly (p<0.0001, as determined by Kruskal-Wallis test), compared to the corresponding values of immobilized beads, with a within-dwell standard deviation of  $0.52~\mu m$  and  $0.80~\mu m$  for beads on the floor and ceiling respectively (Figure 2C).

We also looked at the precision of bead tracking as the bead leaves and returns to the floor and ceiling by taking advantage of the successive up/down motion of the beads. In this assay, each bead dwelled on the ceiling and floor three times each. The positions of each dwell were averaged together to obtain three values for the ceiling, and three for the floor. The standard deviation of the three floor and ceiling values reflects this between-dwells precision and were 0.9 and 2.6  $\mu$ m (Figure 2C). These values were significantly different (p <0.0001) from each other and the corresponding within dwell standard deviations.

# Radial profile modifications to improve bead tracking

Our tracking method utilizes radial profiles generated from the diffraction ring pattern around an off-focus bead image compared to a LUT of reference images to determine the axial position of a bead. We sought to determine if erroneous bead positions are the result of imperfections in the radial profiles. We identified bead traces with worse precision on the ceiling than the floor. An example trace is shown in Figure 3A which has a between-ceiling-dwell of 4.6  $\mu$ m but only 0.34  $\mu$ m for the floor. The within-dwell standard deviation of ceiling positions for this bead ranged from 0.66 to 2.0  $\mu$ m. The corresponding within-dwell standard deviation of floor positions ranged from 0.18 to 0.41  $\mu$ m.

All time points of the six surface dwells were identified (colored points in Figure 3A). The radial profiles from each of these time points were generated and overlaid (Figure 3B). Upon visual inspection we noticed that the overall shapes of the radial profiles lined up well for all beads on the same surface. However, the profiles had discrepancies in the maximum and minimum pixel intensities, and these discrepancies were larger for the ceiling than for the floor profiles.

We hypothesized that pixels with the lowest and highest pixel intensities occurred the same distance from the bead center, and the only variation was the magnitude of the intensity of the maxima and minima. Therefore, all radial profiles were scaled so that the pixel intensities ranged from 0 to 100. A similar process of normalizing the radius vector has been implemented in other works for tracking beads in the z-axis to accommodate for variations in illumination<sup>23,29</sup>. The radial profiles for each surface overlapped better overall but were still not completely aligned (Figure 3C). The pixels closest to the center of the bead still varied in pixel intensity. We developed a method to truncate the radial profiles to remove the pixels closest to the bead center. All pixels from the bead center to a truncation point were excluded from analysis. A single truncation point was identified for all 8.3 µm beads. Using the in-focus images of a sample of 26 beads, we identified the location of the overall minimum in the radial intensity profile for each of these beads (Figure S1). This location sometimes varied slightly between the beads, so the highest frequency minimum-pixel location, the 11<sup>th</sup> pixel from the center, was chosen as the truncation point for all beads of this size.

By truncating and scaling the radial profiles, the new track of the same bead in Figure 3A had clearly more consistent ceiling positions. The within-dwell  $\sigma$  of ceiling positions ranged between 0.43 and 0.66  $\mu$ m and the between-dwell  $\sigma$  of ceiling positions decreased from 2.6 to 0.62  $\mu$ m (Figure 3D).

Modifying Radial Profiles Improves Surface Position Estimations

To characterize the effect of the radial profile modifications, we reanalyzed all bead tracks by (1) just scaling the radial profiles, (2) just truncating the radial profiles, and (3) both scaling and truncating. These modifications were only implemented to determine the axial positions and not the lateral. To evaluate the effect of modifying the radial profile, the changes in tracking precision were analyzed for the data set. The variation within ceiling and floor dwells were determined by looking at the standard deviation of axial positions for all timepoints in a single dwell. The variation between dwells was found from the standard deviation of the average position of each of the three dwells on the ceiling and floor.

All radial profile modifications significantly decreased the standard deviation of positions within a ceiling dwell (p<0.0001) with truncating alone resulting in the largest decrease (Figure 4A). While the beads were on the floor, the standard deviation of positions within dwells was significantly decreased by truncating alone or scaling with truncating the radial profiles (p<0.0001) (Figure 4A). These two modifications resulted in nearly similar average  $\sigma$  values.

When looking at the  $\sigma$  between dwells on the ceiling, the error also significantly decreased with all modifications, with the greatest effect being from scaling with truncating (p<0.0001) (Figure 4B). Scaling with truncating was not significantly different from truncating alone. No modification method generated a significant decrease of the standard deviation between floor dwells (Figure 4B).

## Variation in Bead Velocity

One routine purpose of bead tracking for magnetic tweezer use is to estimate the magnitude of the force being applied to a bead. This is frequently done on each bead because magnetic beads vary in magnetic properties and thus respond differently within a given magnetic field. To estimate the exact force applied to a bead, a modified version of Stoke's Law can be used to estimate force from maximum bead velocity while the beads are pulled by a magnetic field 10,22,30. To characterize the precision of velocity measurements on moving beads, beads were pulled from the chamber ceiling to the floor three times with identical magnetic fields with a force of approximately 5 pN. Any variation between the three velocities for each bead will be largely due to the analysis and is expected to scale with magnitude of the velocity. Therefore, comparison of the normalized error of the velocity measurements can serve as an additional form of error evaluation using axial positions between the chamber surfaces, which have not been considered so far. While we cannot easily compare specific axial positions beyond the chamber ceiling and floor, comparing the bead velocities measured during each pull on the same bead will also give us some insight into the precision of tracking in the middle of the chamber.

To find the velocity, the slope was calculated using a linear regression fit to the positions that fall within the middle third of the chamber (Figure 4C). Beads near surfaces experience higher drags due to changes in fluid flow due to the presence of the surface but within the middle third of the chamber, the effects of the two surfaces are constant, so the standard approach for calibrating magnetic beads is to track in this region and use a correction factor<sup>10,31</sup>. To normalize the error so that the errors of higher velocity beads do not dominate the measurement, we report the fractional standard deviation. The fractional standard deviation was calculated by dividing the standard deviation of the three velocity measurements by the average of the three velocity measurements for each bead (Figure 4D).

The average fractional standard deviation decreased from 0.083 to 0.040 upon scaling and truncating and to 0.058 when just truncating the radial profiles (Figure 4D), both of which

indicate a statistically significant decrease (p<0.001). Scaling, either with or without truncating, did not provide a statistically significant improvement. Therefore, we conclude that truncating the radial profiles significantly improves measurement of bead velocity and thus the calibration of force applied by magnetic beads. Furthermore, it appears that truncation has a positive effect on the entire chamber and not just the chamber ceiling and floor.

Improvement truncation has on tracking precision of moving beads in a different axial region. The beads analyzed so far were collected so that the chamber floor was about 50-60 μm from the focus. We were interested in whether truncation also improved tracking precision at axial locations closer to the focus. Therefore, we collected an additional data set where the chamber floor was about 10 μm away from the focus – a distance that has been associated with optimal precision of measurements <sup>14,17,18</sup>. Figure 5 shows that truncation statistically improves the standard deviation of positions both within and between dwells on the chamber floor, in addition to the fractional standard deviation of velocity. However, the standard deviation of positions within and between dwells on the chamber ceiling did not exhibit significant improvement. This is likely because the chamber ceiling for these measurements is at a similar distance from the focal plane as the chamber floor in Figure 4, which also did not exhibit much improvement from truncation. While this region appears to have minimal benefit from truncation, additional ranges of axial locations appear to greatly benefit from truncation.

 Analysis improvements can be applied to different size beads

We next asked whether truncation was necessary due to some property that is unique to the  $8.3~\mu m$  Bangs Laboratories magnetic beads we initially used or is more generally beneficial. We therefore collected additional tracks of moving beads, using beads of diameter  $2.8~\mu m$  (Dynabeads),  $5.8~\mu m$  (Bangs Laboratories),  $8.8~\mu m$  (Spherotech), and  $11.0~\mu m$  (Spherotech). These tracks were analyzed first without any radial profile modifications (original analysis) and then by truncation. For each bead type, the truncation point was determined from the mode of the location of minimum intensity of the radial profiles for a sample of in-focus beads as described above (Figure S1). The truncation point scaled with the size of the bead: the innermost 8 pixels of the  $2.8~\mu m$  beads, 9 pixels of the  $5.8~\mu m$  beads, 11 pixels for the  $8.8~\mu m$  beads, and 15 pixels for the  $11~\mu m$  beads were removed for truncation.

For all bead sizes, truncation improved both within-dwell (Figure 6A) and between dwell (Figure 6B) variation on the ceiling, and improved or had no significant effect on these variations on the floor. Interestingly, the smaller beads on the floor provided the most precise measurements of all conditions prior to truncation, but truncation was still immensely impactful for increasing precision of measurements on these small beads in all locations.

Furthermore, for all beads analyzed, the velocity measurements were more consistent when the radial profiles were truncated (Figure 6C). The fact that truncation improved velocity measurements for the large beads (Figure 6C) even when it did not improve tracking at the floor between dwells (Figure 6B) suggests that truncation improved tracking in the middle of the chamber. This is noteworthy as measurement of the velocity of a moving bead is commonly used to measure the force on magnetic beads in a magnetic field. Increasing the precision of velocity measurements therefore improves the estimation of force applied by magnetic beads.

In summary, truncation had marked benefits for measuring both position and velocity of all beads tested, and did not exhibit a significant disadvantage in our assays. These results

suggest that truncation of radial profiles should be routinely implemented when tracking beads that are not immobilized.

#### Discussion

Here we address errors that arise in tracking a moving magnetic microsphere by presenting a means to measure these errors and a simple method to minimize these errors. We observed that tracking errors of moving beads were significantly higher when the bead was farther away from the focal plane (Figure 2C) similar to what has been shown for immobilized beads in this work (Figure 2C) and in previous works<sup>14</sup>. However, we found that the error of tracking a moving bead was significantly higher than when tracking a stationary bead, even closer to the focus. Using a high precision z-positioner to follow a moving bead could reduce the discrepancy in error observed at different axial positions, but such a positioner would not remove the error we observed when a bead was mobile compared to immobilized. Furthermore, a positioner would not focus on all beads simultaneously in multiplexing applications in which beads are moving at different speeds or stretching objects to different positions.

Blurring of the radial profiles could contribute to the tracking errors if the beads move significantly within the acquisition time of the camera. Beads are on average held to the bottom surface by 5 pN of force from gravity and the magnetic field in our assay. Using the formula for scale height to calculate H, the average distance from a surface of a particle subjected to thermal energy kT and a constant force F, we estimate that beads are expected to remain around a

characteristic height of  $H = \frac{kT}{F} = 0.8$  nm of the surface. While movement in the lateral plane

may also reduce accuracy, we used a 5 ms acquisition time in this study, during which time an 8 um bead is expected to move less than 10 nm due to diffusion within the lateral plane<sup>32,33</sup>, and even less due to the lateral velocities we measured. This is comparable to the precision of tracking the centroids of immobilized beads in the lateral plane. These calculations make it highly unlikely that blurring is a significant contributor to tracking error in our studies.

Moreover, the tracking errors did not appear as random fluctuations, but rather were highly correlated in time, with sudden changes in calculated axial position occurring occasionally as beads moved across a surface, the magnetic field changed, or when beads left and returned to the same surface. Artifacts caused by the movements of imperfect beads may also explain why some beads have clearly visible artifacts in their tracking and other beads do not. We hypothesize that these errors occur as slightly irregular beads rotate, so irregularities affect the radial profiles in different ways. Presumably, tracking errors may be due to asymmetry in the bead images caused by the optical system. While this is possible in our system, these errors would affect both immobilized and mobile beads and thus would not explain the discrepancy in error between the two bead types.

For all bead sizes, these errors were significantly mitigated by truncating the radial profile to remove pixels closest to the center of the bead, especially in axial regions with the highest errors. We suspect truncating the radial profiles of a bead accommodates for imperfections in the bead geometry which result in highly variable pixel intensities in the center of an off-focus bead image. If a bead cannot rotate, these imperfections would not interfere with LUT comparisons and therefore, truncating the radial profile would not be necessary, and might even remove useful information for estimating the bead's axial position. This illustrates the importance of optimizing and characterizing tracking algorithms in a situation that addresses the full complexity inherent in the experimental condition in which the algorithm will be used.

We also tested whether scaling the radial profiles might help. If the poor tracking was due to sudden but subtle changes in ambient lighting or pixel acquisition time, then normalizing the radial profiles should help. In our case, truncation appeared to help slightly, but the improvement was rarely if ever statistically significant, whether applied to the original or truncated profiles. This suggests that irregularities in lighting or camera function were not significantly affecting our data. The value of scaling therefore remains unclear but may benefit other data sets and did not have a significant disadvantage in our hands.

It may be noted that our measured positions of immobilized beads still had a high standard deviation – over an order of magnitude larger than what was observed for immobilized beads in other works<sup>16</sup>. Because the errors caused by bead movement dwarf the errors in tracking immobilized beads, we do not find it effective to compromise efficiencies in our workflow to optimize tracking on immobilized beads, but it is worth explaining the source of these errors for others' consideration. A major limitation on precision of tracking immobilized beads in this work is the low magnification we used. It has been shown that the error associated with axial bead tracking increases as magnification and numerical aperture decreases<sup>9</sup>, especially below 30x<sup>16</sup>, and the publications reporting low nanometer resolution employed objectives with at least 40x magnification <sup>14,17,18</sup>. Because we are interested in tracking relatively large microbeads (~8 um), we use a 20x objective to maximize the number of beads in a field of view. To further optimize our workflow, the same sample of calibration beads was used to create the LUT for all beads of the same size. In contrast, some studies take calibration images of each analysis bead before applying a magnetic field and use these images to calculate the axial positions of the same bead while moving<sup>9,14,18</sup>. Kovari et al. demonstrated that beads analyzed with a LUT generated from a different bead rather than the same bead decreased the tracking accuracy by over an order of magnitude, resulting in an error of 100-200 nm, comparable to what we observed<sup>23</sup>. An additional source of potential error is that we did not use an immobilized reference bead to subtract instrument drift<sup>9,10</sup>, but instead use a perfect focus system to minimize drift to within 25 nm resolution (Nikon perfect focus system). While precision of immobilized beads could be optimized further, the improvement would be trivial compared to the large error contributed by the mobility of beads.

The modifications in LUT tracking methods we propose here should be broadly useful in biological measurements using magnetic tweezers because LUT is a common method used for 3-dimensional particle tracking due to its flexibility in microscope settings and low computational cost. Tracking of freely moving magnetic beads has been used to calibrate the force on a bead in a magnetic field from the viscous drag<sup>11</sup>, measure the viscoelastic properties of cytoplasm<sup>34,35</sup>, measure the mechanical properties of the nuclear envelope<sup>36</sup>, and the inner cell mass of a mouse embryo<sup>35</sup>. Notably, while it may be possible to minimize rotational asymmetry through manufacturing processes, all types of beads we tested demonstrated significantly lower precisions when moving freely (Figure 6) than when immobilized<sup>10</sup>, and all benefited from this modification of the tracking method (Figure 6). While we were unable to improve the precision to that of an immobilized bead, we found truncating the radial profiles significantly improved the tracking error in most aspects examined. Since truncating the radial profiles is a relatively easy process that does not add much computation time, we highly recommend this modification to be implemented when tracking moving beads.

### **Supporting material**

One video and one figure are included.

504505 Acknowledgements

We would like to thank Dr. Paul Wiggins for his helpful discussions and comments on the manuscript, Dr. Rachel Klevit for additional manuscript comments, and Dr. Keith Johnson for his initial contributions to our magnetic tweezers and bead tracking software. This research was supported by NIH 1R01AI119675 (WET), T32GM008268 (LAC), and NSF CMMI – 1824792 (WET).

511 512

513514

# **Author contributions**

LAC and WET designed research. LAC performed research and analyzed data. LAC and WET wrote the manuscript.

515516

### **Declaration of interests**

The authors declare no competing interests.

518519

517

### References

- Wu M, Roberts JW, Kim S, Koch DL, Delisa MP. Collective Bacterial Dynamics
   Revealed Using a Three-Dimensional Population-Scale Defocused Particle Tracking
   Technique. Appl Environ Microbiol. 2006;72(7):4987-4994. doi:10.1128/AEM.00158-06
- Dulin D, Cui TJ, Cnossen J, Docter MW, Lipfert J, Dekker NH. High Spatiotemporal Resolution Magnetic Tweezers: Calibration and Applications for DNA Dynamics.
   *Biophys J.* 2015;109(10):2113-2125. doi:10.1016/j.bpj.2015.10.018
- 526 3. Löf A, Walker PU, Sedlak SM, et al. Multiplexed protein force spectroscopy reveals equilibrium protein folding dynamics and the low-force response of von Willebrand factor. *Proc Natl Acad Sci.* 2019;116(38):201901794. doi:10.1073/pnas.1901794116
- Bornfleth H, Edelmann P, Zink D, Cremer T, Cremer C. Quantitative motion analysis of subchromosomal foci in living cells using four-dimensional microscopy. *Biophys J*.
   1999;77(5):2871-2886. doi:10.1016/S0006-3495(99)77119-5
- 53. Heinrich V, Wong WP, Halvorsen K, Evans E. Imaging biomolecular interactions by fast three-dimensional tracking of laser-confined carrier particles. *Langmuir*. 2008;24(4):1194-1203. doi:10.1021/la7027059
- Kou L, Jin L, Lei H, et al. Real-time parallel 3D multiple particle tracking with single molecule centrifugal force microscopy. *J Microsc*. 2019;273(3):178-188.
   doi:10.1111/jmi.12773
- 7. Makarchuk S, Beyer N, Gaiddon C, Grange W, Hébraud P. Holographic Traction Force Microscopy. *Sci Rep.* 2018;8(1):1-11. doi:10.1038/s41598-018-21206-2
- 540 8. Zhao X, Zeng X, Lu C, Yan J. Studying the mechanical responses of proteins using magnetic tweezers. *Nanotechnology*. 2017;28(41):414002. doi:10.1088/1361-6528/aa837e
- 9. Ribeck N, Saleh OA. Multiplexed single-molecule measurements with magnetic tweezers. *Rev Sci Instrum.* 2008;79:94301. doi:10.1063/1.2981687
- Johnson KC, Clemmens E, Mahmoud H, Kirkpatrick R, Vizcarra JC, Thomas WE. A multiplexed magnetic tweezer with precision particle tracking and bi-directional force control. *J Biol Eng.* 2017;11(1). doi:10.1186/s13036-017-0091-2
- Kollmannsberger P, Fabry B. High-force magnetic tweezers with force feedback for biological applications. *Rev Sci Instrum*. 2007;78(11):4561. doi:10.1063/1.2804771
- 549 12. Carter BC, Shubeita GT, Gross SP. Tracking single particles: A user-friendly quantitative

- evaluation. *Phys Biol.* 2005;2:60-72. doi:10.1088/1478-3967/2/1/008
- 551 13. Cheezum MK, Walker WF, Guilford WH. Quantitative comparison of algorithms for tracking single fluorescent particles. *Biophys J.* 2001;81(4):2378-2388. doi:10.1016/S0006-3495(01)75884-5
- Zhang Z, Menq C-H. Three-dimensional particle tracking with subnanometer resolution using off-focus images. *Appl Opt.* 2008;47(13):2361-2370. doi:10.1364/AO.47.002361
- Lee S-H, Roichman Y, Yi G-R, et al. Characterizing and tracking single colloidal particles
   with video holographic microscopy. *Opt Express*. 2007;15(26):18275.
   doi:10.1364/oe.15.018275
- Van Loenhout MTJ, Kerssemakers JWJ, De Vlaminck I, Dekker C. Non-bias-limited
   tracking of spherical particles, enabling nanometer resolution at low magnification.
   *Biophys J.* 2012;102(10):2362-2371. doi:10.1016/j.bpj.2012.03.073
- 562 17. Brouwer TB, Hermans N, van Noort, J1. Brouwer, T.B., N. Hermans and J van N 2020. 563 MN 3D T of MU an F-PABJ 118:2245–2257. oh. Multiplexed Nanometric 3D Tracking 564 of Microbeads Using an FFT-Phasor Algorithm. *Biophys J.* 2020;118(9):2245-2257. 565 doi:10.1016/j.bpj.2020.01.015
- Cnossen JP, Dulin D, Dekker NH. An optimized software framework for real-time, high-throughput tracking of spherical beads. *Rev Sci Instrum*. 2014;85(10):0-10.
   doi:10.1063/1.4898178
- Del Rio A, Perez-Jimenez R, Liu R, Roca-Cusachs P, Fernandez JM, Sheetz MP.
   Stretching single talin rod molecules activates vinculin binding. *Science* (80-).
   2009;323(5914):638-641. doi:10.1126/science.1162912
- Rief M, Gautel M, Oesterhelt F, Fernandez JM, Gaub HE. Reversible unfolding of
   individual titin immunoglobulin domains by AFM. *Science* (80-). 1997;276(5315):1109 1112. doi:10.1126/science.276.5315.1109
- Forero M, Yakovenko O, Sokurenko E V, Thomas WE, Vogel V. Uncoiling mechanics of
   Escherichia coli type I fimbriae are optimized for catch bonds. *PLoS Biol*.
   2006;4(9):1509-1516. doi:10.1371/journal.pbio.0040298
- Haber C, Wirtz D. Magnetic tweezers for DNA micromanipulation. *Rev Sci Instrum*.
   2000;71(12):4561-4570. doi:10.1063/1.1326056
- Kovari DT, Dunlap D, Weeks ER, Finzi L. Model-free 3D localization with precision estimates for brightfield-imaged particles. *Opt Express*. 2019;27(21):29875-29895.
   doi:10.1364/oe.27.029875
- Parthasarathy R. Rapid, accurate particle tracking by calculation of radial symmetry centers. *Nat Methods*. 2012;9(7):724-726. doi:10.1038/nmeth.2071
- Abraham A V, Ram S, Chao J, Ward ES, Ober RJ. Quantitative study of single molecule location estimation techniques. *Opt Express*. 2009;17(26):23352-23373.
- http://www4.utsouthwestern.edu/wardlab/EstimationTool. Accessed November 18, 2020.
- Lansdorp BM, Tabrizi SJ, Dittmore A, Saleh OA. A high-speed magnetic tweezer beyond 10,000 frames per second. *Rev Sci Instrum*. 2013;84(4):0-5. doi:10.1063/1.4802678
- 590 27. Ghosh RN, Webb WW. Automated detection and tracking of individual and clustered cell surface low density lipoprotein receptor molecules. *Biophys J.* 1994;66(5):1301-1318. doi:10.1016/S0006-3495(94)80939-7
- 593 28. Carlucci L, Johnson KC, Thomas WE. Three dimensional bead tracking. 2021. doi:10.5281/zenodo.4724130
- 595 29. Cheng P, Jhiang SM, Menq CH. Real-time visual sensing system achieving high-speed 3D

- 596 particle tracking with nanometer resolution. *Appl Opt.* 2013;52(31):7530-7539.
   597 doi:10.1364/AO.52.007530
- Yago K. THE MECHANICAL AND COLLOIDAL PROPERTIES OF AMOEBA
   PROTOPLASM A N D THEIR RELATIONS TO THE MECHANISM OF AMOEBOID
   MOVEMENT. Comp Biochem Physiol. 1961;3:77-91.
- Maude AD. End effects in a falling-sphere viscometer. *Br J Appl Phys*. 1961;12:293-295.
   https://iopscience.iop.org/article/10.1088/0508-3443/12/6/306/pdf. Accessed August 29,
   2019.
- 604 32. Chio CC, Tse Y-LS. Hindered Diffusion near Fluid-Solid Interfaces: Comparison of Molecular Dynamics to Continuum Hydrodynamics. 2020. doi:10.1021/acs.langmuir.0c01228
- Goldman AJ, Cox RG, Brenner H. Slow viscous motion of a sphere parallel to a plane wall-Motion through a quiescent fluid. *Chem Eng Sci.* 1967;22(4):653-660. doi:10.1016/0009-2509(67)80048-4
- Bausch AR, Möller W, Sackmann E. Measurement of local viscoelasticity and forces in living cells by magnetic tweezers. *Biophys J.* 1999;76(1 I):573-579. doi:10.1016/S0006-3495(99)77225-5
- Wang X, Luo M, Wu H, et al. A Three-Dimensional Magnetic Tweezer System of Intraembryonic Navigation and Measurement. *IEEE Trans Robot*. 2018;34(1):240-247.
- Wang X, Ho C, Tsatskis Y, et al. Intracellular manipulation and measurement with multipole magnetic tweezers. *Sci Robot*. 2019;4. doi:10.1126/scirobotics.aav6180

## **Figure Legends**

617 618 619

620

621

622 623

624

625

626 627

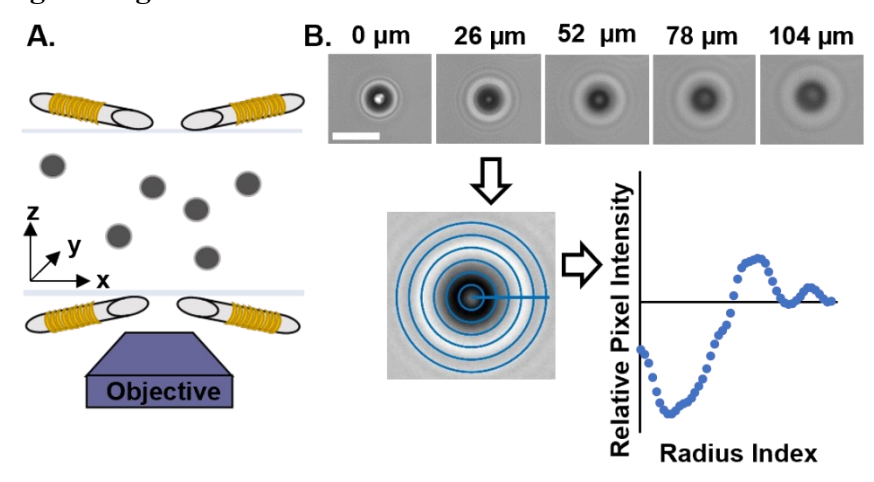


**Figure 1.** (A) Illustration of a magnetic tweezers with electromagnets. Magnetic beads (gray circles) are manipulated by electromagnets positioned above and below a chamber. A microscope objective views the beads from below the chamber. (B) View of magnetic beads from the microscope objective with beads at different distances below a relative focal point. Scale bar =  $20 \mu m$  (73 pixels). Radial profiles are generated by radial projection in which pixels evenly spaced from the center are averaged together.

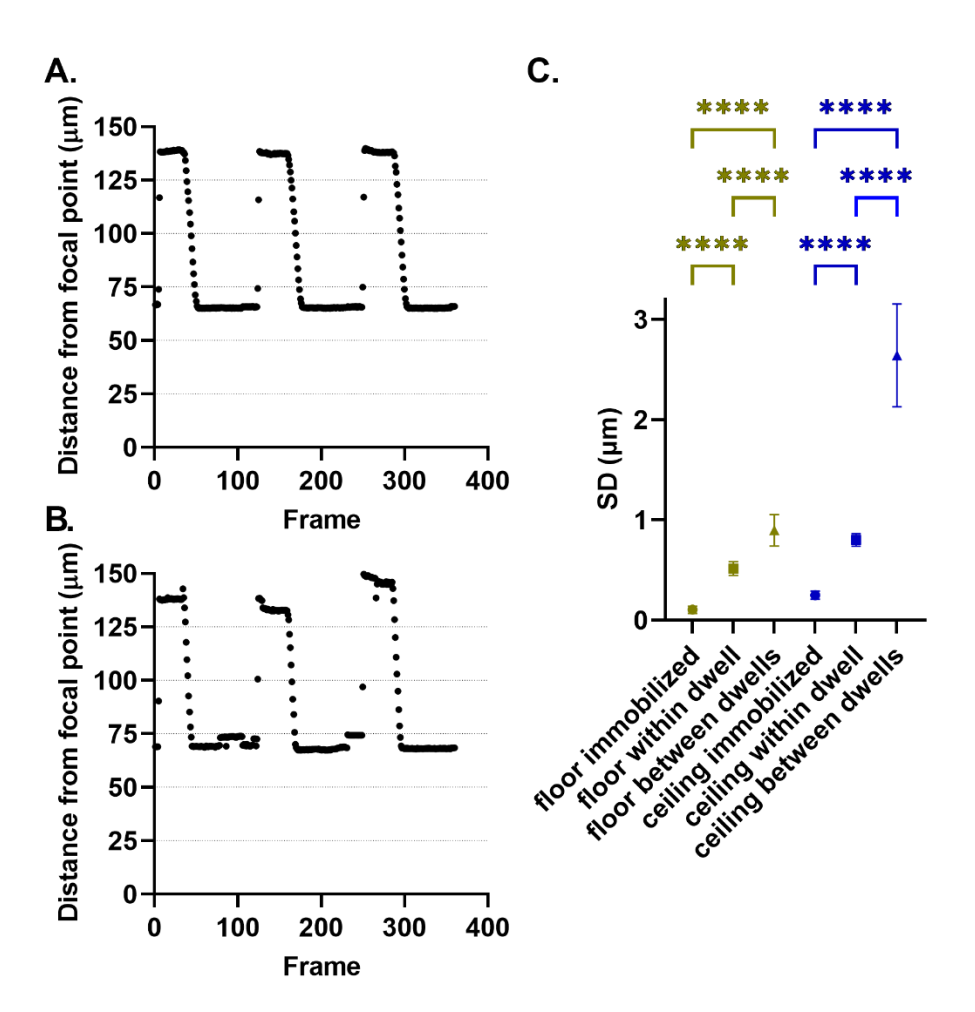


**Figure 2.** To characterize the accuracy of the tracking method beads were successively pulled to the top and bottom of the chamber (A) Example of an ideal trace where the bead stops moving at consistent z-positions, indicating consistent estimation of the ceiling and floor of the chamber. (B) Example of a clearly erroneous trace in which the positions of the chamber ceiling and floor are inconsistent. (C)  $\sigma$  of positions on the floor and ceiling when beads were immobilized,  $\sigma$  of positions within each dwell, and  $\sigma$  of average position of dwells for each bead. Values indicate average  $\sigma$  and error bars indicate 95% confidence intervals. \*\*\*\* p<0.0001 as determined by Kruskal-Wallis test.

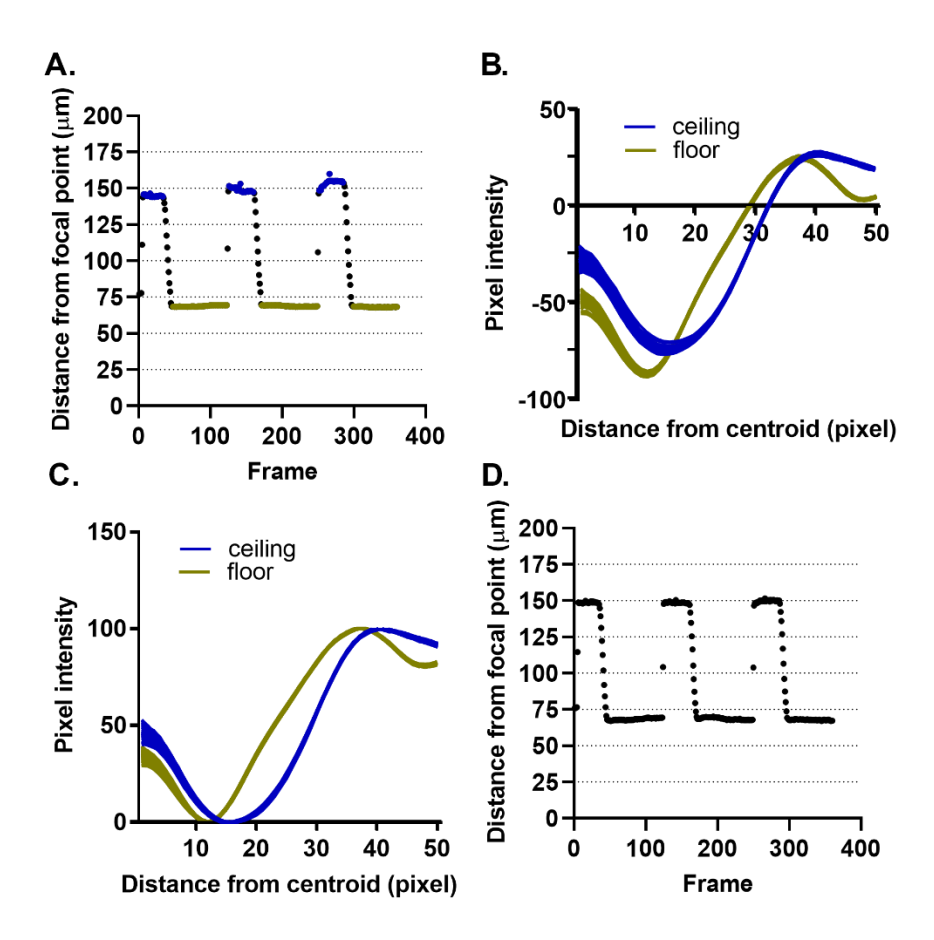


**Figure 3.** Modifications to radial profiles can remedy apparent tracking inaccuracies. (A) z-position vs frame plot of example bead exhibiting varying ceiling estimation. Colored points indicate when bead was identified to be on a chamber surface (B). Overlay of radial profiles of bead from (A) when on the chamber ceiling and floor. Regions where the overlay is thicker indicates higher variability between radial profiles. (C) Overlay of radial profiles from (B) after radial vectors have been scaled. Greyed box indicates region of radial profile truncated from z-position analysis. (D) z-positions of bead from (A) after all radial profiles have been scaled and truncated.

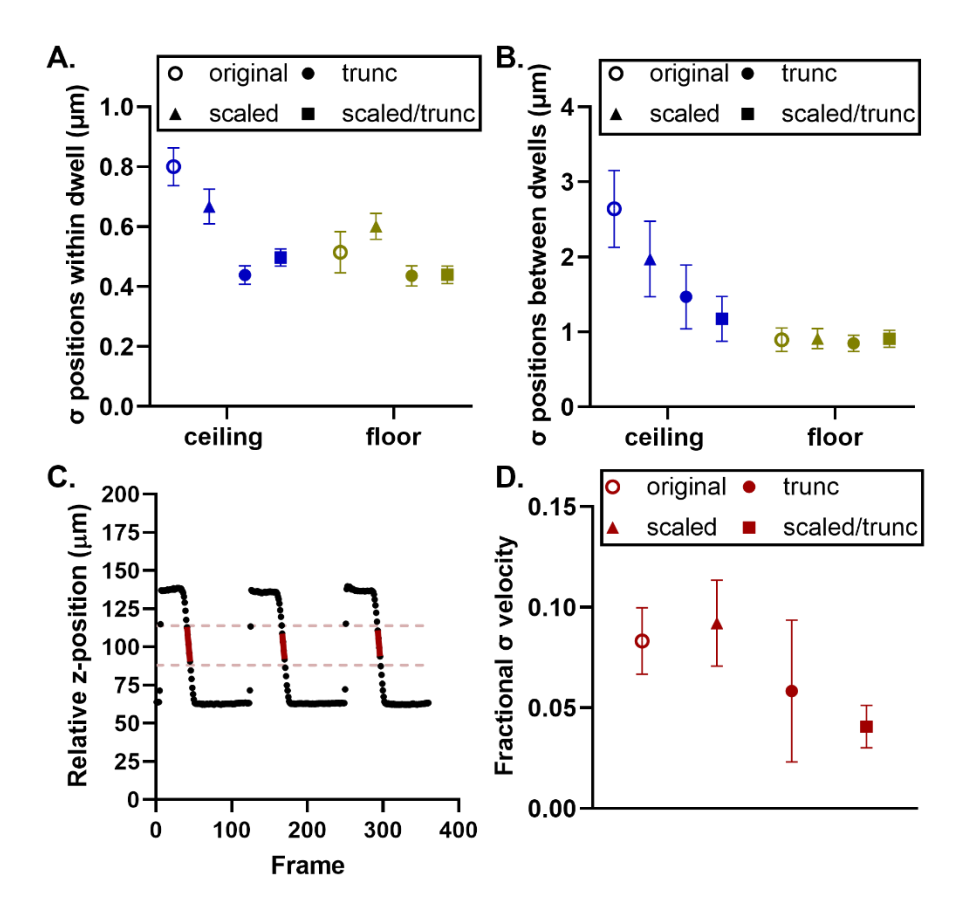


**Figure 4.** (A)  $\sigma$  of axial positions of ceiling and floor measurements within a single dwell. (B)  $\sigma$  of average ceiling and floor positions between 3 dwells. (C) The downward velocity of a moving bead is calculated by fitting a linear regression to the determined bead positions as the bead travels through the middle third region of the chamber. (D) The fractional  $\sigma$ , found by dividing the standard deviation of the three velocity measurements by the average velocity, is used to evaluate the precision of the velocity measurements. Values indicate average  $\sigma$  and error bars indicate 95% confidence intervals.

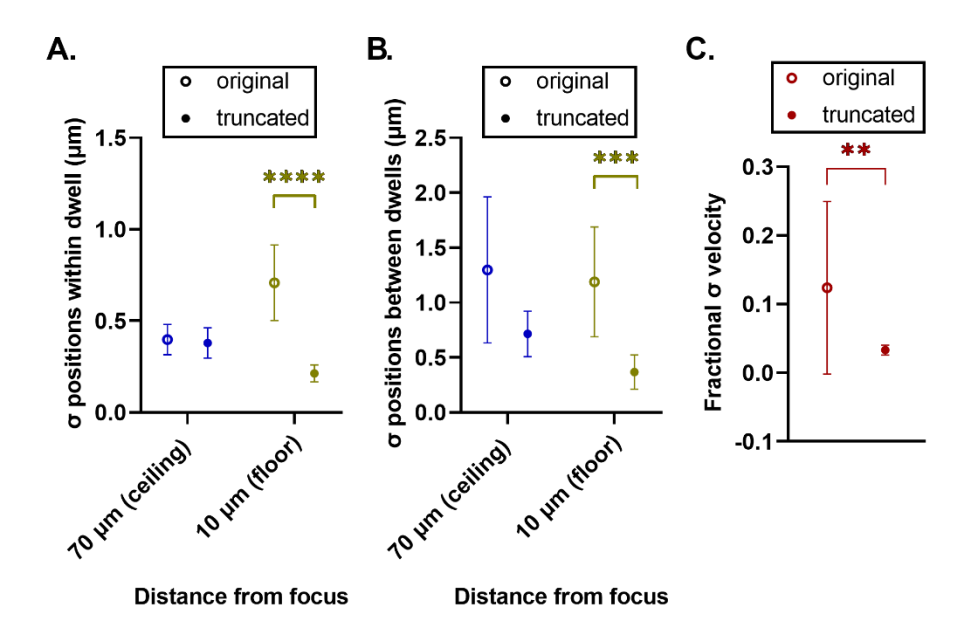


**Figure 5.** Improvement truncation of radial profiles has on tracking 8.3  $\mu$ m beads closer to the focus.  $\sigma$  of ceiling and floor positions (A) within dwell, and (B) between dwells (C) The fractional  $\sigma$  of velocity. Values indicate average  $\sigma$  and error bars indicate 95% confidence intervals, \*\*p<0.01, \*\*\*p<0.001 as determined by Wilcoxon signed rank test.

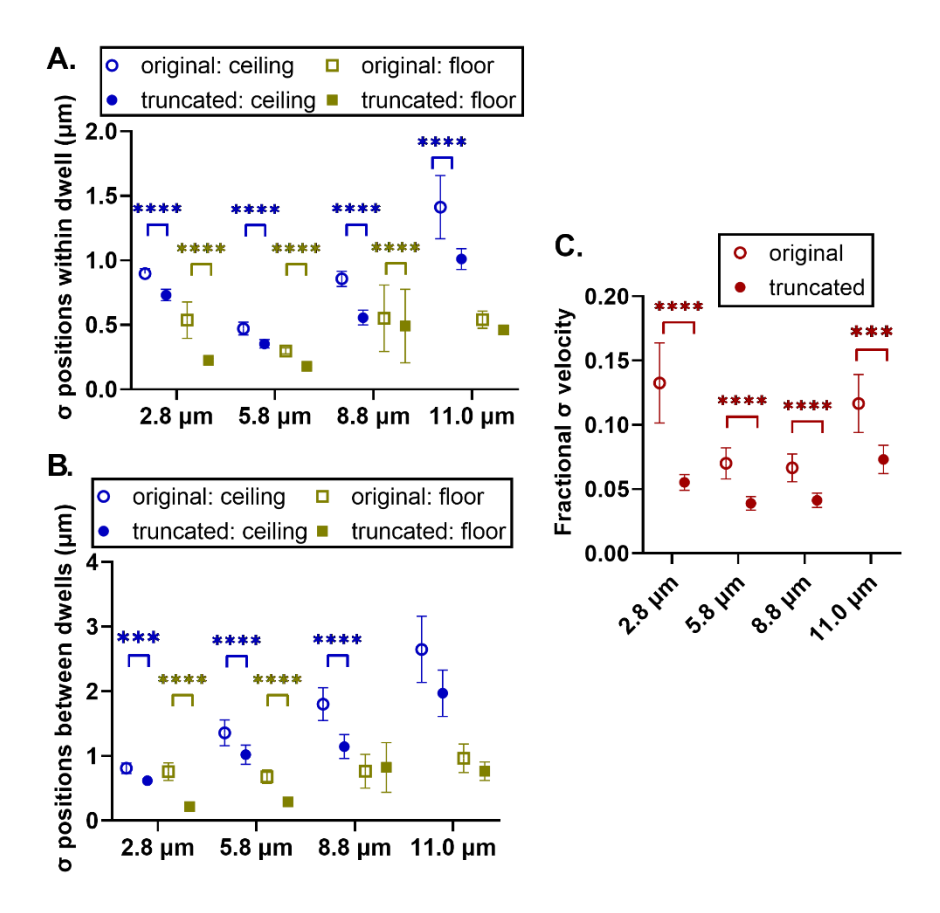


**Figure 6.** Improvement truncating radial profiles have on beads of various sizes. (A)  $\sigma$  of axial positions of ceiling and floor measurements within a dwell (B)  $\sigma$  of average ceiling and floor between 3 dwells (C) Fractional  $\sigma$  of velocity \*\*p<0.01, \*\*\*p<0.001, \*\*\*\*p<0.0001 as determined by Wilcoxon signed rank test. Values indicate average  $\sigma$  and error bars indicate 95% confidence intervals.